

# Drag-guided diffusion models for vehicle image generation

Nikos Aréchiga, Frank Permenter, Chenyang Yuan\*  
Toyota Research Institute  
firstname.lastname@tri.global

Binyang Song  
Massachusetts Institute of Technology  
binyangs@mit.edu

June 19, 2023

## Abstract

Denosing diffusion models trained at web-scale have revolutionized image generation. The application of these tools to engineering design is an intriguing possibility, but is currently limited by their inability to parse and enforce concrete engineering constraints. In this paper, we take a step towards this goal by proposing physics-based guidance, which enables optimization of a performance metric (as predicted by a surrogate model) during the generation process. As a proof-of-concept, we add drag guidance to Stable Diffusion, which allows this tool to generate images of novel vehicles while simultaneously minimizing their predicted drag coefficients.

## 1 Introduction

Diffusion models have produced state of the art results for high-resolution image generation. One powerful aspect of diffusion models is the incorporation of *text-based guidance*, which steers the image generation process towards an output that matches a user-provided description. Such guidance is implemented in DALL-E 2 [25], Imagen [30] and Stable Diffusion [27]. Given their capabilities, it is natural to ask how current image generation tools can be applied to engineering design, and, in particular, if text-guidance is sufficient to specify quantitative engineering constraints. Simple experiments reveal significant challenges. For example, given a text prompt of “a house with *two* windows”, a text-guided diffusion model produces a house with windows, but ignores the quantitative constraint on the specified *number* of windows (Figure 1a). The prompt “a car with a drag coefficient of 0.5” is also completely misinterpreted (Figure 1b), showing an inability of the generation process to even correctly parse the constraint.

To successfully incorporate engineering constraints into existing image generation tools, it is clear that new guidance approaches must be developed. In this paper, we implement *physics-based* guidance that simultaneously estimates and optimizes the performance of the generated object. As a proof-of-concept, we implement *drag* optimization of *vehicles*, but our approach can be adapted to any design task that admits a *surrogate model* of performance with the following characteristics:

1. The input is an image, as produced by a diffusion process for image generation.

---

\*Authors listed alphabetically



(a) “a house with two windows”



(b) “a car with a drag coefficient of 0.5”

Figure 1: Illustrates the inability of text-guidance to realize quantitative design specifications. Images were generated by `craiyon.com`

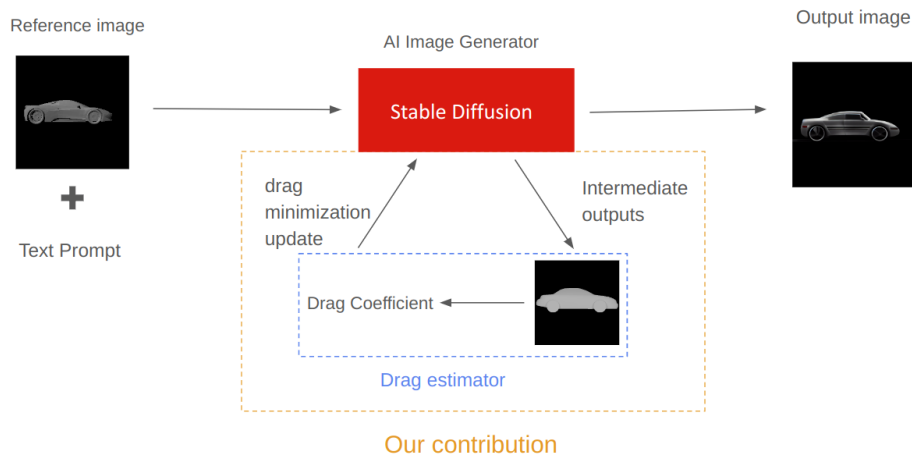


Figure 2: Our pipeline for incorporating drag minimization into diffusion models.

2. The model is robust to distributional shifts in the input.
3. The model is differentiable, allowing for gradient-based optimization of the output.

For the task of vehicle drag optimization, we train a surrogate model that meets these specifications using the dataset [31], which consists of two-dimensional (2D) vehicle renderings labeled with drag coefficients calculated from fluid-dynamics simulations. Aiming for robustness to distributional shifts, we build our model using feature-space embeddings from widely used object recognition networks [23, 12, 9]. Finally, our model is implemented using a deep-neural network and is hence differentiable.

Leveraging our surrogate model, we integrate *drag guidance*<sup>1</sup> into Stable Diffusion (Figure 2), and show that this integrated system can generate car images that both match a text prompt and minimize predicted drag. We also find that drag guidance can produce more aesthetically streamlined outputs. Figure 3 contains illustrative examples of our results compared to baseline images generated by an unmodified version of Stable Diffusion.

<sup>1</sup>In this paper, we use “drag” and “drag coefficient” interchangeably.

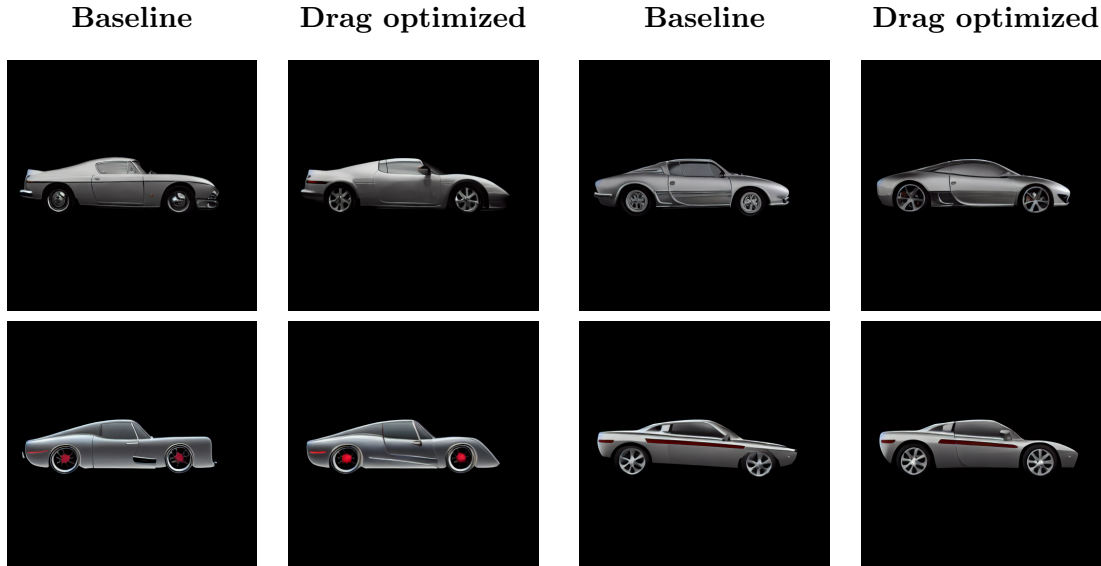


Figure 3: Outputs of Stable Diffusion with and without our drag-guidance technique.

## 2 Related Work

**Guided diffusion** Guidance aims to minimize an auxiliary loss function  $\phi(x)$  during the image generation process [3]. This is done by incorporating the gradient of  $\phi(x)$  into each generation step. Guidance techniques can be differentiated by the type of loss function. In *classifier-based* guidance [8], the loss function  $\phi(x)$  is the logit probability of a specified class in a pre-trained classifier. The aim of this guidance is to steer the output towards this class. In *text-based* guidance,  $\phi(x)$  is a similarity score computed in a latent space, e.g., the cosine similarity between the CLIP embedding of the image  $x$  and a given text-prompt [23, 7, 20, 15]. Guidance can also be used to solve linear equations  $Ax = b$  by setting  $\phi(x) = \|b - Ax\|^2$ . This setup generalizes image inpainting, compressed sensing, and super-resolution [6, 5]. Alternatively, one can implement *classifier-free* guidance, in which gradients of  $\phi(x)$  are effectively learned during training. Such approaches have been used for text guidance [13], inpainting [27] and single-view reconstruction [17].

**Diffusion for design** Prior applications of diffusion to engineering design include [11, 18], which train *new* diffusion models for a specific design task. In contrast, our work focuses on adapting an *existing* diffusion model (Stable Diffusion), aiming to leverage the web-scale dataset used for its training.

**Drag optimization and machine learning** Drag optimization is a classical problem that can be solved using PDE-optimization techniques. These approaches require accurate solutions of the Navier-Stokes equations, which are computationally expensive to obtain and sensitive to shape representation. Circumventing these difficulties using ML-techniques is an active area of research. One thread of research replaces direct solution of the Navier-Stokes equations with a *surrogate model*. These models are trained using computational fluid-dynamics (CFD) simulations and either predict pressure or velocity fields [34, 26, 2, 10, 4, 1], and/or a performance measure (e.g., drag coefficient) directly from model parameters [31, 4]. Different model architectures have been used, including Gaussian process regression [34], graph neural networks [2, 10], geodesic convolu-

tional neural networks [4, 1], variational autoencoders (VAEs) [29], and UNets [33, 14]. Our work continues this thread and develops a surrogate model for drag coefficient estimation using *linear regression* on features extracted from pretrained neural-networks. Another thread concerns novel shape representations that maintain end-to-end differentiability when cascaded with a surrogate model. Such representations include Deep Implicit Fields [26], PolyCubes [34], and 2D renderings [28, 33, 14, 31]. Our work uses 2D renderings proposed by [31], which capture the point-wise depth and normal information of three dimensional (3D) shapes using RGB color channels of pixel data. This image representation allows us to easily implement a differentiable surrogate-model that can predict drag coefficients directly from intermediate Stable Diffusion outputs.

### 3 Denoising Diffusion Models

Diffusion models are a class of generative models inspired by the physical process of diffusion. These models are trained by adding progressively larger amounts of Gaussian noise to a given data set, mimicking a diffusion process. Sampling reverses this process through *denoising*.

#### 3.1 Training

Diffusion models estimate a *noise vector*  $\epsilon \in \mathbb{R}^n$  from a given  $y \in \mathbb{R}^n$  and *noise level*  $\sigma > 0$  such that  $y = x + \sigma\epsilon$  approximately holds for some  $x$  in the training set. The learned estimator, denoted  $\epsilon_\theta : \mathbb{R}^n \times \mathbb{R}_+ \rightarrow \mathbb{R}^n$ , is called a *denoiser*. The trainable parameters, denoted jointly by  $\theta \in \mathbb{R}^m$ , are found by (approximately) minimizing

$$L(\theta) := \mathbb{E}_{x, \sigma, \epsilon} \|\epsilon_\theta(x + \sigma\epsilon, \sigma) - \epsilon\|^2 \quad (1)$$

when  $x$  is drawn from the training-set distribution,  $\sigma$  is drawn uniformly from a finite set of positive numbers, and  $\epsilon$  is drawn from a Gaussian distribution  $\mathcal{N}(0, I)$ .

Current state-of-the-art diffusion models modify this training process in a few ways. Models supporting classifier-free text guidance add text embeddings (from CLIP, for example) to the denoiser input [23]. Models supporting high-resolution image synthesis implement *latent diffusion* [27], i.e., the variable  $x$  is not an element of pixel space, but, rather, an element of a lower-dimensional latent space defined by a VAE.

#### 3.2 Sampling

Let  $\{\sigma_t\}_{t=0}^T$  denote a set of noise levels  $\sigma$  used in training and assume that  $\sigma_t > \sigma_{t-1}$ . The sequence  $\sigma_t$  is used by *sampling algorithms* to construct novel images using a trained denoiser  $\epsilon_\theta$ . We use the DDIM sampler [32] which, given  $x_T \sim \mathcal{N}(0, \sigma_T^2 I)$ , generates an image  $x_0$  via the following recursion<sup>2</sup>

$$x_{t-1} = x_t - (\sigma_t - \sigma_{t-1})\epsilon_\theta(x_t, t). \quad (2)$$

Classifier-free text-guidance [13] executes this recursion using a modified denoiser  $\epsilon_\theta(x_t, t, y)$  that takes a reference latent embedding  $y$  (e.g., from CLIP) as an optional third input. Concretely, it constructs  $\epsilon_\theta(x_t, t)$  via

$$\epsilon_\theta(x_t, t) = (1 - w)\epsilon_\theta(x_t, t, \emptyset) + w(\epsilon_\theta(x_t, t, y)) \quad (3)$$

where  $w$  is a weighing factor and  $\emptyset$  denotes the empty string.

<sup>2</sup>We note [32] presents this recursion in coordinates  $z_t := \sqrt{\alpha_t}x_t$  where  $\alpha_t$  satisfies  $\sigma_t^2 = (1 - \alpha_t)/\alpha_t$ .

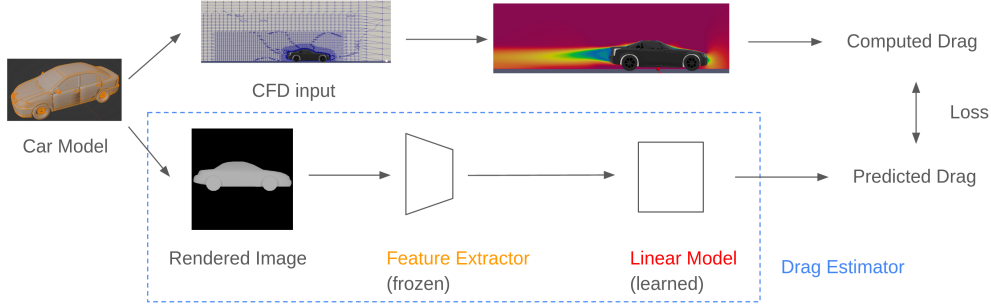


Figure 4: Training the drag estimator

Features	Dimension	Train $R^2$	Test $R^2$	Test MSE
CLIP	512	0.639	0.545	0.00251
ViT	768	0.639	0.549	0.00249
ResNet	2048	0.630	0.509	0.00271
Random	2560	0.640	0.554	0.00246

Table 1: Performance of drag estimator with different feature extractors.

## 4 Method and Implementation

In this section, we first describe the construction of a surrogate model for drag coefficient estimation. We then describe our technique for drag guidance, which incorporates gradients of this model into the sampling process.

### 4.1 A surrogate model for drag estimation

To estimate drag, we train a surrogate model that predicts drag coefficients from side-view vehicle images (Figure 4). Training uses the dataset [31], which consists of 2D vehicle renderings labeled with drag coefficients calculated from CFD simulations. Our model consists of a trainable linear-layer attached to a frozen feature extractor, a well-established technique in transfer learning for improving robustness to out-of-distribution shifts [16]. More details of the training process can be found in Section 4.3. Table 1 compares model performance for different feature extractors, specifically, CLIP [23], ResNet [12], Vision Transformers [9], and random convolutions [24].

Note that the surrogate model alone is not sufficient to perform drag optimization: starting with an image of a car and minimizing the predicted drag in pixel space produces results similar to Figure 5a. We remedy this using guided diffusion, which will interleave drag minimization steps with denoising steps.

### 4.2 Drag-guided diffusion

Let  $\phi_{\text{drag}} : \mathbb{R}^{C \times H \times W} \rightarrow \mathbb{R}$  denote our surrogate model. To implement drag-guided diffusion, we follow [8, Algorithm 2] and modify the sampling step (2) to

$$x_{t-1} = x_t - (\sigma_t - \sigma_{t-1})(\epsilon_\theta(x_t, t) + \eta_t \nabla \phi_{\text{drag}}(\hat{x}_0^t)), \quad (4)$$

where  $\eta_t$  denotes an iteration-dependent weight and  $\hat{x}_0^t$  denotes the denoised output, defined as  $\hat{x}_0^t = x_t - \sigma_t \epsilon_\theta(x_t, t)$ . Per [21], we can interpret construction of  $\hat{x}_0^t$  as approximate projection onto

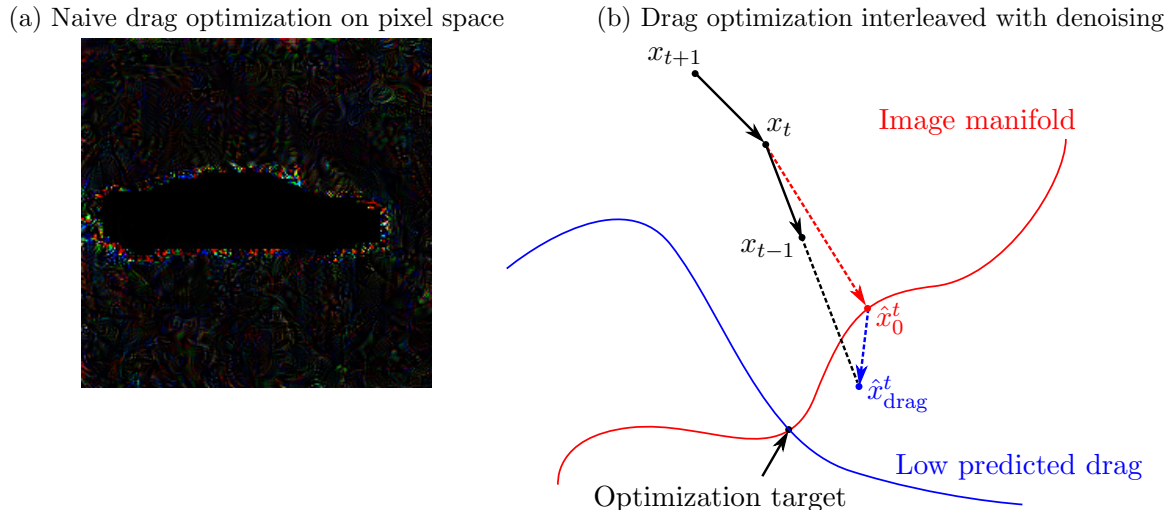


Figure 5: An illustration of how drag guidance works. Noisy images produced by naively minimizing the surrogate model (Figure 5a) are avoided by the inclusion of denoising steps (Figure 5b).

the image manifold. The iterations (4) in turn can be reinterpreted as a damped form of projected gradient descent, an algorithm that alternates between projection and gradient steps. Precisely, (4) implicitly constructs a shadow iterate  $\hat{x}_{drag}^t$  using a projected-gradient descent iteration, and then dampens the update to  $\hat{x}_{drag}^t$  using the quantity  $\alpha_t := 1 - \sigma_{t-1}/\sigma_t$ . Consider the following.

**Proposition 4.1.** *The iterations (4) are equivalent to*

$$\begin{aligned} \hat{x}_0^t &= x_t - \sigma_t \epsilon_\theta(x_t, t) \\ \hat{x}_{drag}^t &= \hat{x}_0^t - \gamma_t \nabla \phi_{drag}(\hat{x}_0^t) \\ x_{t-1} &= (1 - \alpha_t)x_t + \alpha_t \hat{x}_{drag}^t \end{aligned} \tag{5}$$

where  $\alpha_t = 1 - \frac{\sigma_{t-1}}{\sigma_t}$  and  $\gamma_t = \sigma_t \eta_t$ .

*Proof.* Expanding and simplifying the last equation gives

$$\begin{aligned} x_{t-1} &= (1 - \alpha_t)x_t + \alpha_t [x_t - \sigma_t \epsilon_\theta(x_t, t) - \gamma_t \nabla \phi_{drag}(\hat{x}_0^t)] \\ &= x_t + \alpha_t [\sigma_t \epsilon_\theta(x_t, t) - \gamma_t \nabla \phi_{drag}(\hat{x}_0^t)]. \end{aligned}$$

Equating with (4) shows that  $\sigma_t - \sigma_{t-1} = \alpha_t \sigma_t$  and  $(\sigma_t - \sigma_{t-1})\eta_t = \alpha_t \gamma_t$ . Rearranging proves the claim.  $\square$

In total, we can interpret construction of  $\hat{x}_0^t$  as stepping towards the image manifold, and construction of  $\hat{x}_{drag}^t$  as a drag-minimization step. This is illustrated by Figure 5b.

### 4.3 Implementation details

To train our model, we used side-view renderings from the dataset [31]. For each item in this dataset, we randomly generated 10 new training examples using horizontal flips, vertical shifts (up to 25 pixels) and jitter (up to five percent) in brightness, contrast, saturation and hue. The

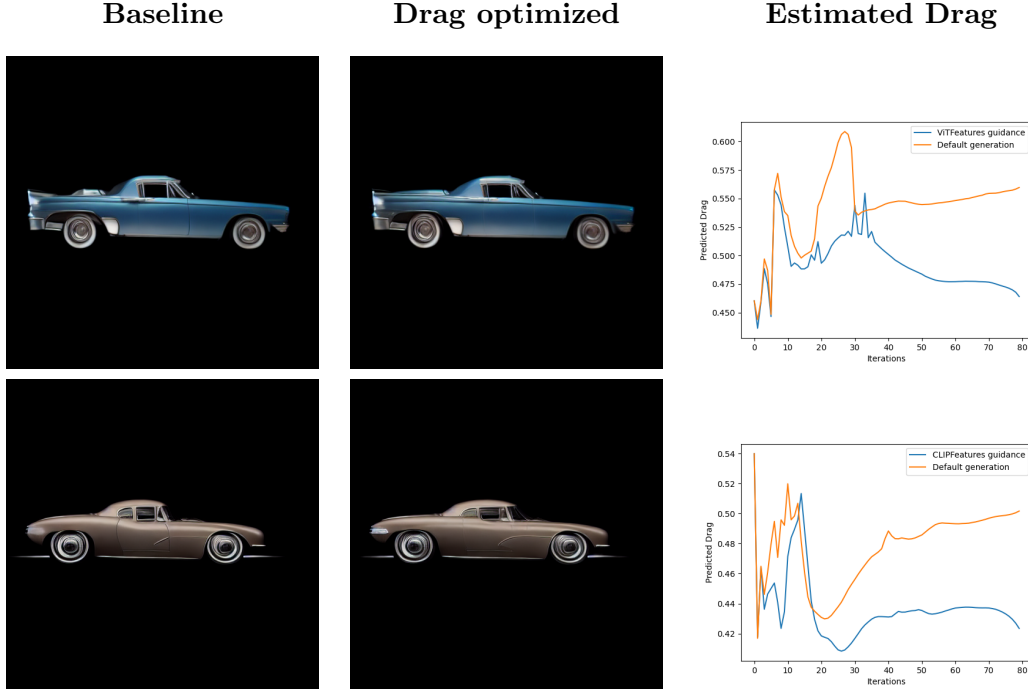


Figure 6: Outputs of our image generation pipeline with drag optimization, compared to baseline images with the drag optimization turned off.

renderings were also resized to 224 by 224 pixels to match the input size of the pretrained feature extractors, which we obtained from the following Huggingface repositories:

`openai/clip-vit-base-patch32`, `google/vit-base-patch16-224-in21k`, `microsoft/resnet-50`.

We also compared performance to random convolutional features, which we constructed using a kernel size of five and weights drawn from a standard normal distribution. At the output of these convolutions, we applied a bias of +2, a ReLU nonlinearity, and a pooling operation using a 55 by 55 window. After extracting the features, we use ridge regression with regularization parameter  $\lambda = 100$  and  $\lambda = 10$ , for the pretrained and random features respectively, to train the last linear layer.

Finally, drag guidance was incorporated into a checkpoint of Stable Diffusion available at `runwayml/stable-diffusion-v1-5`, with  $\eta_t = \eta_0 / \sqrt{1 + 1/\sigma_t^2}$ , and  $\eta_0 = 400$ . During sampling, we fix a reference image  $x_0$ , which is a side-view rendering of a car, and set  $T = 80$ . Then we let  $x_T = x_0 + \sigma_T \epsilon$ , where  $\epsilon \sim \mathcal{N}(0, I)$ , a commonly used technique in image-to-image generation [19]. We also fix a text prompt and use a scale of 7.5 for classifier-free text guidance.

## 5 Experimental Results

### 5.1 Generation of novel designs

We first consider generation of novel vehicle images with drag guidance. Compared to baseline generation, we find that drag guidance can change the generated image in subtle ways (e.g. artifact removal or surface smoothing as in Figure 6) or through significant redesigns (e.g. adding a roof to a convertible as in Figure 8). In all cases, however, a coherent vehicle shape is preserved, as is the

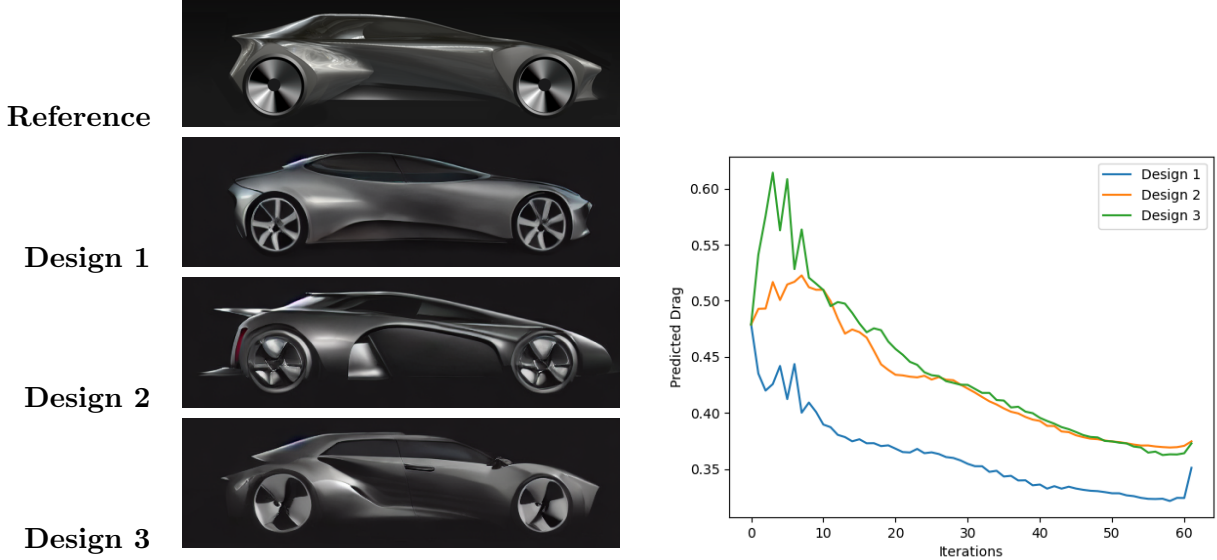


Figure 7: Drag-guided redesigns of a reference image.

artistic style, showing that text-based guidance can work in concordance with drag optimization. Sample results are shown in Figure 3 and Figure 6. Figure 6 also confirms that drag guidance indeed decreases predicted drag. Appendix A contains more examples.

## 5.2 Drag-guided redesign

Recall that the DDIM sampler is initialized via  $x_T = x_0 + \sigma_T \epsilon$ , where  $x_0$  denotes a provided reference image and  $\epsilon \sim \mathcal{N}(0, I)$ . Deviation of the DDIM output from  $x_0$  is controlled by the size of the noise-level  $\sigma_T$ . For  $\sigma_T$  sufficiently small, the deviation preserves the basic structure of  $x_0$ . This leads to drag-guided *redesigns* of the reference. Figure 7 illustrates redesigns produced by this procedure. Note that for each redesign, the initial predicted drag is the same and equal to the predicted drag of the reference image.

## 5.3 Drag-guided diffusion with a gradient-estimation sampler

A recent variation on DDIM is based on reinterpreting sampling as approximate gradient-descent on the Euclidean distance function of the training set [21]. This leads to a gradient-estimation (GE) sampler that averages  $\epsilon_\theta(x_t, t)$  over multiple time-steps, exploiting the fact that the gradient of the distance function is constant along gradient-descent trajectories [21, Section 4]. To use this sampler, one replaces  $\epsilon_\theta(x_t, t)$  in (4) with  $\gamma \epsilon_\theta(x_t, t) + (1 - \gamma) \epsilon_\theta(x_{t+1}, t + 1)$  for chosen  $\gamma \in \mathbb{R}$ . We compare outputs between GE and DDIM samplers in Figure 8 using  $\gamma = 2$ .

## 5.4 Distributional robustness of drag estimator

Our drag estimator  $\phi_{\text{drag}}$  should generalize to the set of intermediate denoised images  $\hat{x}_0^t := x_t - \sigma_t \epsilon_\theta(x_t, t)$  generated by the diffusion process. There are two forms of distributional shift that inhibit good generalization. First, the dataset used to train the denoiser  $\epsilon_\theta$  differs from the dataset used to train  $\phi_{\text{drag}}$ . Second, the distribution of the denoised outputs  $\hat{x}_0^t$  differs from that of the  $\epsilon_\theta$ -training set, given that the denoiser is imperfect, i.e., given that  $\epsilon \neq \epsilon_\theta(x + \sigma_t \epsilon, t)$ . While it is difficult to evaluate this first type of distributional shift, robustness to the second type can be evaluated with

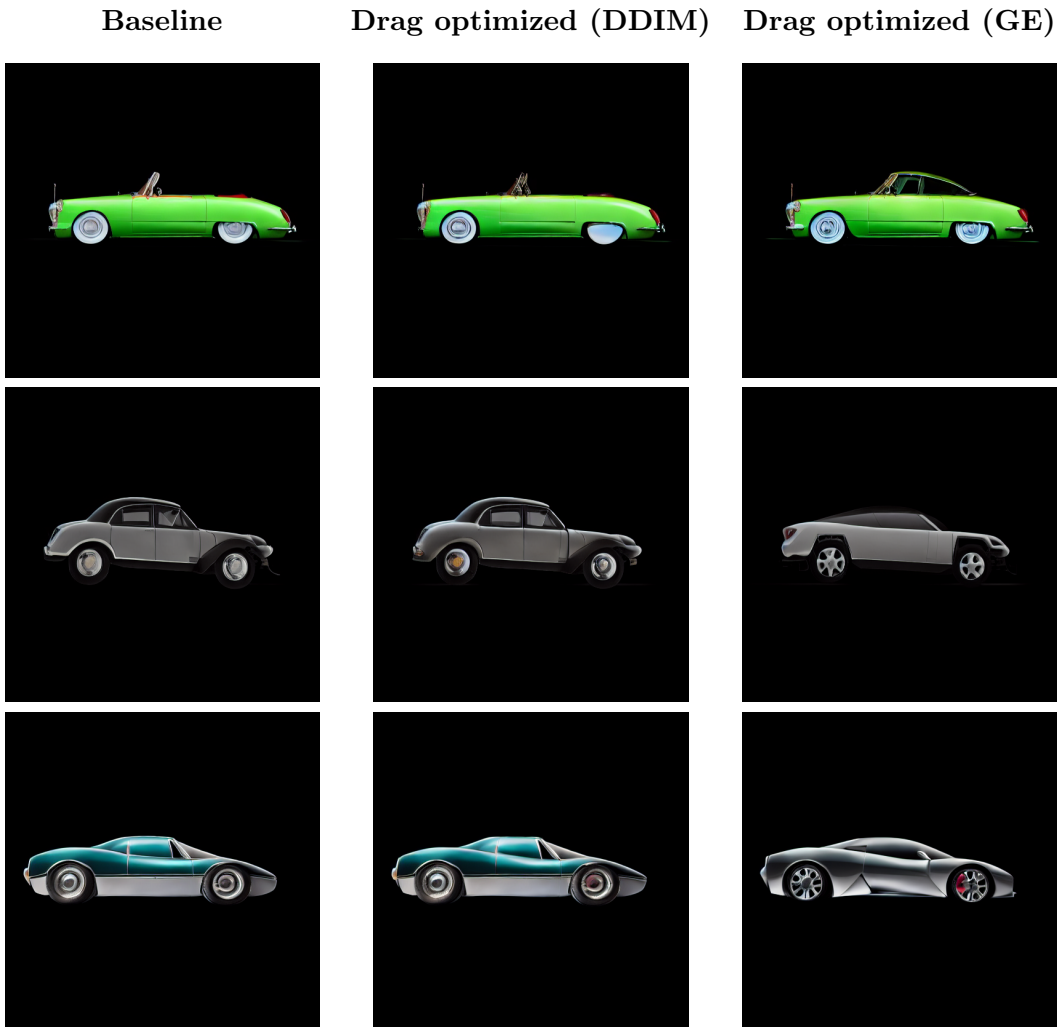


Figure 8: Comparison of DDIM and the gradient-estimation (GE) sampler

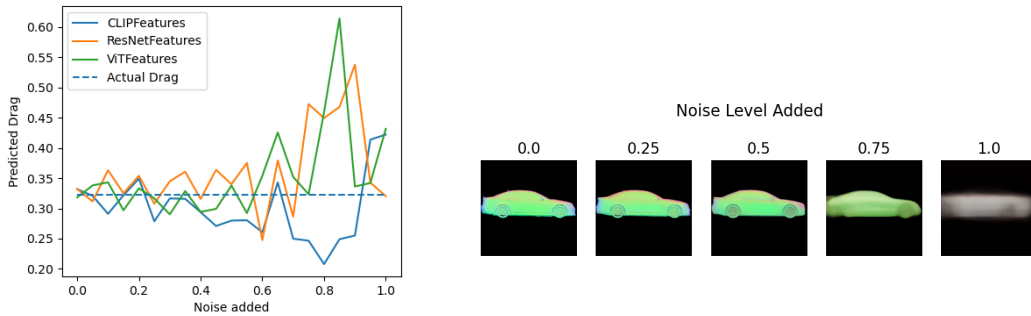


Figure 9: Drag estimator performance on out of distribution data:  $\hat{x}_0^t$  with varying amount of noise added to a single image.

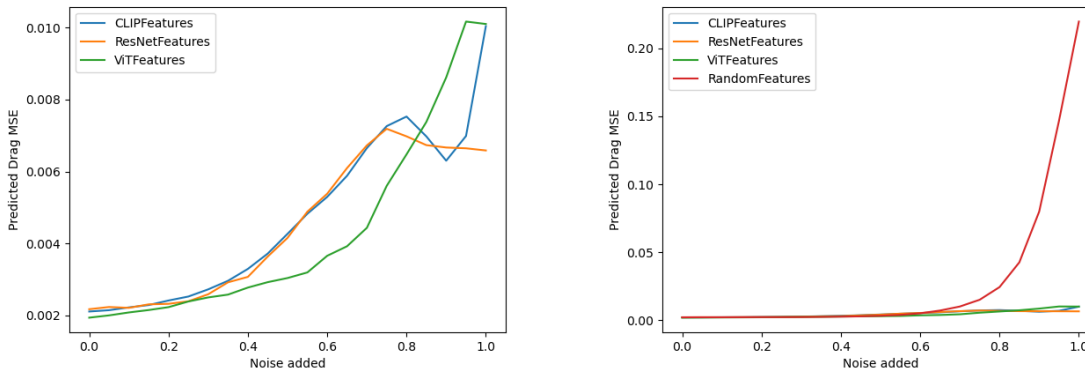


Figure 10: Drag estimator performance on out of distribution data as measured by mean-squared error on the entire dataset. The left plot is a “zoomed-in” version of the right plot, showing that random features leads to a much higher generalization error than features from pre-trained neural networks.

controlled experiments. We carry out two such experiments to evaluate the robustness of  $\phi_{\text{drag}}$  as a function of the chosen feature extractor (Section 4.1). We also note that the first type of shift may be mitigated by retraining  $\phi_{\text{drag}}$  using vehicle images from the Stable Diffusion training set, but defer this to future research.

In our first experiment, we take an image used to train  $\phi_{\text{drag}}$  and add varying levels of noise. We then predict the drag of the different denoised images  $\hat{x}_0^t$ . A visualization of  $\hat{x}_0^t$  and drag predictions for different noise levels on a single example image is shown in Figure 9. We see that the drag estimator can over or underestimate the predicted drag, and that the error increases with the magnitude of added noise. Next, we perform the same experiment over the entire training dataset, and plot the results in Figure 10. The generalization error is measured with the predicted mean-squared-error of the drag coefficient, which increases with the amount of noise added. We see that the features obtained from pretrained neural networks generalize much better than the random features, even though they have similar performance on the training data.

## 6 Conclusion, Limitations and Future Work

Generative AI tools that can synthesize engineering constraints and performance metrics could rapidly speed-up the design process. This work is a step towards building such tools and illustrated, as a proof of concept, that current image generation techniques can be modified to optimize aerodynamic drag. Other performance metrics that can be inferred from images could be incorporated using appropriate modifications.

A current limitation of our pipeline is its difficulty controlling—or even measuring—the error of the surrogate model on the final drag-optimized output, since the ground-truth drag coefficient is not uniquely determined nor computable from the generated 2D rendering. Future work could alter our approach in a few ways to obtain a unique ground truth. For instance, one could formulate the problem completely in 2D by replacing our surrogate model—which predicts 3D drag from a 2D rendering—with a model that predicts 2D drag from a planar car. Alternatively, one can formulate the problem completely in 3D by replacing Stable Diffusion with a 3D generative model. Another limitation of our approach is its 2D image domain formulation, which may limit its design applications. Replacing images with CAD or 3D models is a natural next step. We note combining parametric 3D-models with image diffusion models is the central task of *score distillation sampling* [22]. Adding physics-based guidance to this technique is an interesting topic for future research.

Despite unavailability of ground-truth, there are instances when inaccuracy of the surrogate model is evident. For example, in Figure 11, the surrogate model predicts dramatically different drag coefficients for two cars with similar outlines. Furthermore, the predicted coefficient for one of the cars is negative, which is not physically valid. To improve accuracy, future work could develop active learning techniques that augment the training set by computing ground-truth drag coefficients for generated vehicles. In addition, one could investigate surrogate models with an implicit physical bias that, for instance, only return non-negative drag coefficients and always make similar predictions for similar shapes.

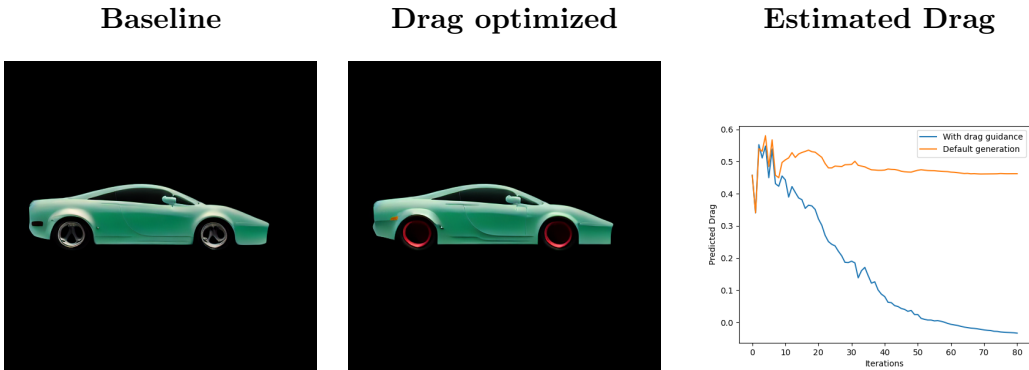


Figure 11: Images generated with and without drag guidance that demonstrate incorrect predictions from the surrogate model. While the car outline is largely unmodified by guidance, the surrogate model predicts large improvements and even negative drag coefficients in the final iterations (blue).

## Acknowledgements

The authors thank Faez Ahmed for several useful discussions.

## References

- [1] A. Abbas, A. Rafiee, M. Haase, and A. Malcolm. Geometrical deep learning for performance prediction of high-speed craft. *Ocean Engineering*, 258:111716, 2022.
- [2] K. R. Allen, T. Lopez-Guevara, K. Stachenfeld, A. Sanchez-Gonzalez, P. Battaglia, J. Hamrick, and T. Pfaff. Physical design using differentiable learned simulators. *arXiv preprint arXiv:2202.00728*, 2022.
- [3] A. Bansal, H.-M. Chu, A. Schwarzschild, S. Sengupta, M. Goldblum, J. Geiping, and T. Goldstein. Universal guidance for diffusion models. *arXiv preprint arXiv:2302.07121*, 2023.
- [4] P. Baque, E. Remelli, F. Fleuret, and P. Fua. Geodesic convolutional shape optimization. In *International Conference on Machine Learning*, pages 472–481. PMLR, 2018.
- [5] H. Chung, J. Kim, M. T. Mccann, M. L. Klasky, and J. C. Ye. Diffusion posterior sampling for general noisy inverse problems. *arXiv preprint arXiv:2209.14687*, 2022.
- [6] H. Chung, B. Sim, D. Ryu, and J. C. Ye. Improving diffusion models for inverse problems using manifold constraints. *arXiv preprint arXiv:2206.00941*, 2022.
- [7] K. Crowson. CLIP guided diffusion, 2021. URL [https://colab.research.google.com/drive/12a\\_Wrfi2\\_gwwAuN3VvMTwVMz9TfqctNj](https://colab.research.google.com/drive/12a_Wrfi2_gwwAuN3VvMTwVMz9TfqctNj).
- [8] P. Dhariwal and A. Nichol. Diffusion models beat GANs on image synthesis. *Advances in Neural Information Processing Systems*, 34:8780–8794, 2021.
- [9] A. Dosovitskiy, L. Beyer, A. Kolesnikov, D. Weissenborn, X. Zhai, T. Unterthiner, M. Dehghani, M. Minderer, G. Heigold, S. Gelly, et al. An image is worth 16x16 words: Transformers for image recognition at scale. *arXiv preprint arXiv:2010.11929*, 2020.
- [10] N. Durasov, A. Lukoyanov, J. Donier, and P. Fua. Debosh: Deep bayesian shape optimization. *arXiv preprint arXiv:2109.13337*, 2021.
- [11] G. Giannone and F. Ahmed. Diffusing the optimal topology: A generative optimization approach. *arXiv preprint arXiv:2303.09760*, 2023.
- [12] K. He, X. Zhang, S. Ren, and J. Sun. Deep residual learning for image recognition. In *Proceedings of the IEEE conference on computer vision and pattern recognition*, pages 770–778, 2016.
- [13] J. Ho and T. Salimans. Classifier-free diffusion guidance. *arXiv preprint arXiv:2207.12598*, 2022.
- [14] S. J. Jacob, M. Mrosek, C. Othmer, and H. Köstler. Deep learning for real-time aerodynamic evaluations of arbitrary vehicle shapes. *arXiv preprint arXiv:2108.05798*, 2021.
- [15] G. Kim, T. Kwon, and J. C. Ye. DiffusionCLIP: Text-Guided Diffusion Models for Robust Image Manipulation. 10 2021. doi: 10.48550/arxiv.2110.02711. URL <https://arxiv.org/abs/2110.02711v6>.
- [16] A. Kumar, A. Raghunathan, R. Jones, T. Ma, and P. Liang. Fine-tuning can distort pretrained features and underperform out-of-distribution. *arXiv preprint arXiv:2202.10054*, 2022.
- [17] R. Liu, R. Wu, B. Van Hoorick, P. Tokmakov, S. Zakharov, and C. Vondrick. Zero-1-to-3: Zero-shot one image to 3d object. *arXiv preprint arXiv:2303.11328*, 2023.
- [18] F. Mazé and F. Ahmed. Topodiff: A performance and constraint-guided diffusion model for topology optimization. *arXiv preprint arXiv:2208.09591*, 2022.
- [19] C. Meng, Y. He, Y. Song, J. Song, J. Wu, J.-Y. Zhu, and S. Ermon. Sdedit: Guided image synthesis and editing with stochastic differential equations. In *International Conference on Learning Representations*, 2021.

- [20] A. Nichol, P. Dhariwal, A. Ramesh, P. Shyam, P. Mishkin, B. McGrew, I. Sutskever, and M. Chen. GLIDE: Towards Photorealistic Image Generation and Editing with Text-Guided Diffusion Models. 12 2021. doi: 10.48550/arxiv.2112.10741. URL <https://arxiv.org/abs/2112.10741v3>.
- [21] F. Permenter and C. Yuan. Interpreting and improving diffusion models using the Euclidean distance function. *arXiv preprint arXiv:2306.04848*, 2023.
- [22] B. Poole, A. Jain, J. T. Barron, and B. Mildenhall. Dreamfusion: Text-to-3d using 2d diffusion. *arXiv preprint arXiv:2209.14988*, 2022.
- [23] A. Radford, J. W. Kim, C. Hallacy, A. Ramesh, G. Goh, S. Agarwal, G. Sastry, A. Askell, P. Mishkin, J. Clark, et al. Learning transferable visual models from natural language supervision. In *International conference on machine learning*, pages 8748–8763. PMLR, 2021.
- [24] A. Rahimi and B. Recht. Random features for large-scale kernel machines. *Advances in neural information processing systems*, 20, 2007.
- [25] A. Ramesh, P. Dhariwal, A. Nichol, C. Chu, and M. Chen. Hierarchical text-conditional image generation with clip latents. *arXiv preprint arXiv:2204.06125*, 2022.
- [26] E. Remelli, A. Lukoianov, S. Richter, B. Guillard, T. Bagautdinov, P. Baque, and P. Fua. Meshsdf: Differentiable iso-surface extraction. *Advances in Neural Information Processing Systems*, 33:22468–22478, 2020.
- [27] R. Rombach, A. Blattmann, D. Lorenz, P. Esser, and B. Ommer. High-resolution image synthesis with latent diffusion models. In *Proceedings of the IEEE/CVF Conference on Computer Vision and Pattern Recognition*, pages 10684–10695, 2022.
- [28] N. Rosset, G. Cordonnier, R. Duval, and A. Bousseau. Interactive design of 2d car profiles with aerodynamic feedback. In *Computer Graphics Forum*, volume 42, 2023.
- [29] S. Saha, T. Rios, L. L. Minku, B. V. Stein, P. Wollstadt, X. Yao, T. Back, B. Sendhoff, and S. Menzel. Exploiting generative models for performance predictions of 3d car designs. In *2021 IEEE Symposium Series on Computational Intelligence (SSCI)*, pages 1–9. IEEE, 2021.
- [30] C. Saharia, W. Chan, S. Saxena, L. Li, J. Whang, E. Denton, S. K. S. Ghasemipour, B. K. Ayan, S. S. Mahdavi, R. G. Lopes, et al. Photorealistic text-to-image diffusion models with deep language understanding. *arXiv preprint arXiv:2205.11487*, 2022.
- [31] B. Song, C. Yuan, N. Arechiga, F. Permenter, and F. Ahmed. Surrogate modeling of car drag coefficient with depth and normal rendering. In *Proceedings of the ASME 2023 IDETC/CIE*, 2023.
- [32] J. Song, C. Meng, and S. Ermon. Denoising diffusion implicit models. *arXiv preprint arXiv:2010.02502*, 2020.
- [33] N. Thuerey, K. Weissenow, L. Prantl, and X. Hu. Deep learning methods for reynolds-averaged navier–stokes simulations of airfoil flows. *AIAA Journal*, 58(1):25–36, 2020.
- [34] N. Umetani and B. Bickel. Learning three-dimensional flow for interactive aerodynamic design. *ACM Transactions on Graphics (TOG)*, 37(4):1–10, 2018.

## A Additional examples

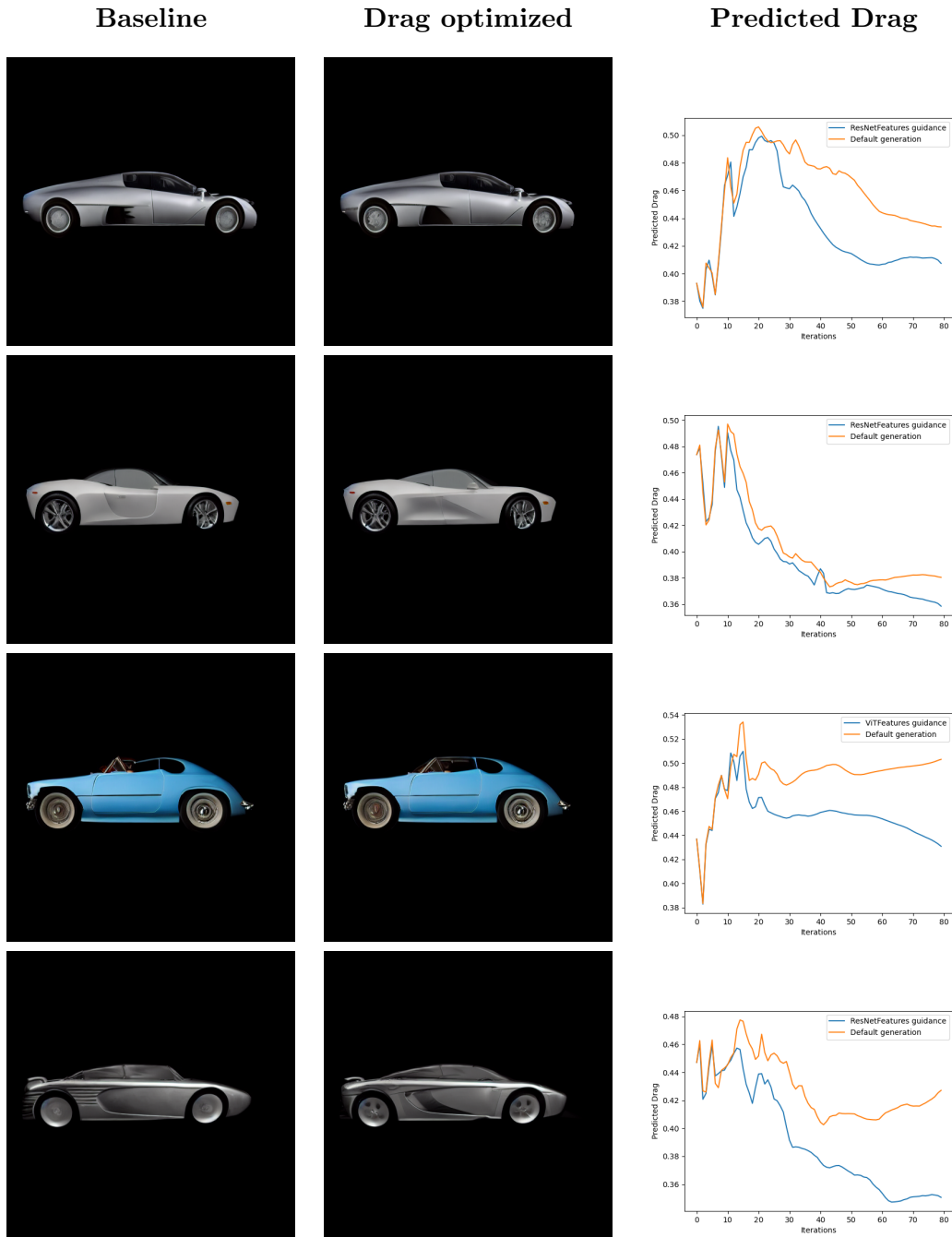


Figure 12: Images generated from the prompt “A car, high resolution studio photo, side view” with and without drag optimization. We also plot drag coefficients predicted by the surrogate model.



Figure 13: Images generated from the prompt “An old fashioned car, high resolution studio photo, side view” with and without drag optimization. We also plot drag coefficients predicted by the surrogate model.

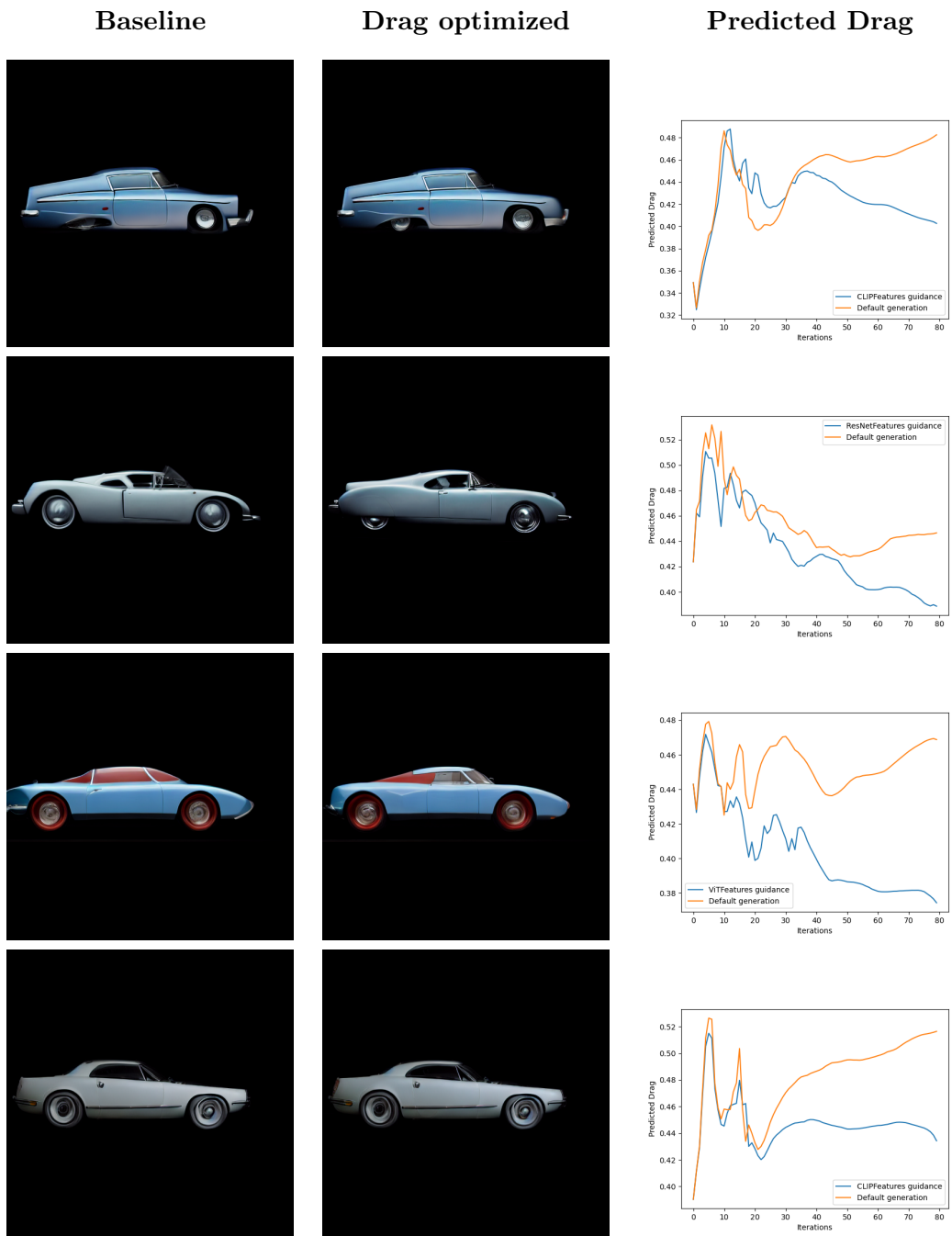


Figure 14: Images generated from the prompt “An iconic car, high resolution studio photo, side view” with and without drag optimization. We also plot drag coefficients predicted by the surrogate model.